

# Influence of chirp, jitter and relaxation oscillations on laser pulse interference in optical quantum random number generator

**ROMAN SHAKHOVOY<sup>1,2\*</sup>, VIOLETTA SHAROGLAZOVA<sup>1,2,3</sup>, ALEXANDER UDALTSOV<sup>1,2</sup>, ALEXANDER DUPLINSKIY<sup>1,2,4</sup>, VLADIMIR KUROCHKIN<sup>1,2</sup>, AND YURY KUROCHKIN<sup>1,2,5</sup>**

<sup>1</sup>*Russian Quantum Center, 45 Skolkovskoye shosse, Moscow, Russian Federation*

<sup>2</sup>*QRate, 100 Novaya str., Skolkovo, Russian Federation*

<sup>3</sup>*Skolkovo Institute of Science and Technology, 30/1 Bolshoy Boulevard, Moscow, Russian Federation*

<sup>4</sup>*Moscow Institute of Physics and Technology, 9 Institutskiy per., Dolgoprudny, Russian Federation*

<sup>5</sup>*NTI Center for Quantum Communications, National University of Science and Technology MISiS, 4 Leninsky prospekt, Moscow, Russian Federation*

*\*r.shakhovoy@goqrate.com*

**Abstract:** The combined effect of chirp and jitter is crucial when elaborating quantum random number generator (QRNG) based on the interference of laser pulses. The chirp is one of the sources of classical noise in the QRNG; therefore, its contribution should be reduced. Here, we consider in detail the interference of gain-switched semiconductor laser pulses affected by the chirp, jitter and relaxation oscillations. It is shown how to reduce the combined impact of chirp and jitter on the interference using a telecom bandpass filter. Experimental results are reproduced by Monte-Carlo simulations using a rigorous model based on the solution of laser rate equations.

## 1. Introduction

The last decade, a large number of studies has been devoted to quantum random number generators (QRNGs) employing the noise of semiconductor lasers. A number of ways to convert phase fluctuations of laser radiation into amplitude modulation that directly provides random bits have been proposed [1-7]. The arrangement with the interference of laser pulses was first proposed in [4], where the train of optical pulses entered into the unbalanced Mach-Zehnder interferometer, whose delay line was chosen in such a way that the corresponding delay time was a multiple of the pulse repetition period. The idea was that at the output of the interferometer one will observe the interference of pulses emitted by the laser at different moments of time. An important requirement for the operation of such a scheme is that the laser should be modulated over the lasing threshold, i.e., after each pulse the laser should be switched to the amplified spontaneous emission (ASE) mode. Since most transitions in the ASE mode are spontaneous, phase correlations of the electromagnetic field are destroyed very quickly, such that each new laser pulse appears with a random phase and the result of their interference becomes a random quantity.

Despite its convenience, the interference of laser pulses has a number of unpleasant features, which adversely affect the visibility of the interference and have an impact on the appearance of the probability density function (PDF) of the random interference signal. This is particularly true for standard telecom lasers, which are usually not well suited for interferometric applications. The most crucial features in such lasers are the inevitable chirping of laser frequency under direct modulation and significant fluctuations of the pulse emission time (jitter).

The combined influence of these two effects in the context of QRNG was considered in [8], where authors demonstrated that the PDF of the interference signal for chirped laser pulses differs markedly from the PDF measured in the absence of chirp. The authors proposed a simple model assuming that laser pulses have a Gaussian shape and exhibit a linear chirp

that allowed them to derive an analytical expression for the interference signal. The main disadvantage of their model is an assumption of uniform PDF for the jitter needed to fit theoretical results to experimental data. However, distribution of pulse emission time fluctuations can be shown to be quite close to Gaussian in case of gain-switched lasers [9] and usually has the rms of the order of 10-50 ps [10, 11]. More detailed investigation reveals that the appearance of the PDF of the interference signal with more realistic jitter is different from the one observed in [8], so the laser pulse interference model should be refined and expanded.

In the present work, we use a more rigorous model taking into account relaxation oscillations in addition to jitter and chirp. Moreover, we consider separately cases with linear and non-linear gain, i.e. take into account both transient and adiabatic chirp. The combined influence of all three effects is considered by solving laser rate equations, so expression for the interference signal in this case cannot be found analytically. Although lack of analytical formulas complicates the analysis of theoretical results, such an approach allows describing the interference of laser pulses distorted by relaxation oscillations and helps explaining the change of the PDF of the interference signal after cutting off the high-frequency part of the laser spectrum with optical bandpass filter.

In the next section, we provide a brief theoretical background for the laser pulse interference and for the effects of jitter, chirp and relaxation oscillations. In section 3, we provide the main theoretical results – Monte-Carlo simulations of the PDF of the interference signal for five different approximations. Related experimental results are given in section 4.

## 2. Theoretical background

### 2.1 Laser pulse interference

Let us consider the laser pulse interference measured using a Michelson fiber optic interferometer (Fig. 1). The delay line  $\Delta L$  in the long arm of the interferometer is chosen so that the corresponding delay time defined by  $\Delta T = 2\Delta L n_g / c$  is multiple of the pulse repetition period  $2\pi/\omega_p$ , such that at the output of the interferometer the  $i$ -th laser pulse of the sequence meets the  $i + N_p$ -th pulse, where  $N_p$  is the number of pulses that have time to pass the short arm of the interferometer during the time needed for the pulse to pass the long arm (here  $c$  is the light speed in vacuum and  $n_g$  is the group index).

In the following, subscripts 1 and 2 will be used to designate the short and long arms of the interferometer, respectively, and to designate laser pulses coming from the respective arms. Assuming that the interfering pulses are polarized in the same plane, i.e. their electric fields can be represented as scalar functions of time, the intensity of the signal at the output of the interferometer can be written as follows:

$$S(t) \sim |E_1(t) + E_2(t)|^2, \quad (1)$$

where  $E_1$  and  $E_2$  are electric fields in the first and second pulses, respectively. The time dependence of the electric field in a pulse can be written in the following form:

$$E_{1,2}(t) \sim \sqrt{P_{1,2}(t)} e^{i\phi_{1,2}(t)}, \quad (2)$$

where  $\phi_{1,2}(t)$  is the phase of the field and  $P_{1,2}(t)$  is the output power in the corresponding pulse. The power of the interfering pulses can be related to the laser output power as follows:

$$\begin{aligned} P_1(t) &= (1 - \alpha_1) T_{01} T_{10} P(t), \\ P_2(t) &= (1 - \alpha_2) T_{02} T_{20} P(t), \end{aligned} \quad (3)$$

where  $\alpha_1$  and  $\alpha_2$  stand for the losses in the optical fiber in the short and long arms of the interferometer, respectively, and  $T_{kl}$  is a coupler transmittance from the input port  $k$  to the output port  $l$  (see Fig. 1).

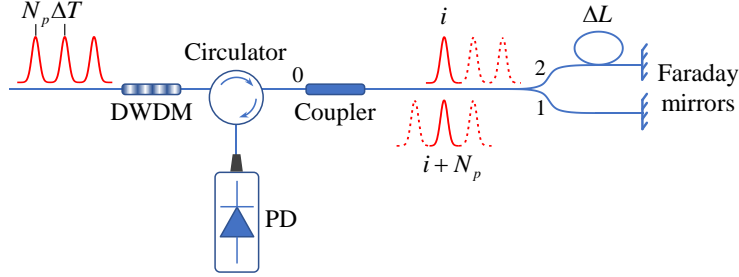


Fig. 1. The optical scheme used in this work to observe interference of laser pulses. The circulator is used to separate optical signals that travel in opposite directions and thus to prevent unwanted feedback into a laser. PD stands for the photodetector; DWDM – dense wavelength division multiplexing bandpass filter.  $\Delta T$  and  $\Delta L$  are defined in the text.

The phase  $\varphi(t)$  of the electric field in the pulse can be written as follows:

$$\varphi(t) = \varphi_p + \int_0^t \omega(t') dt', \quad (4)$$

where  $\omega$  is the angular frequency and  $\varphi_p$  is the initial phase of the pulse at the output of the laser. Denoting central frequency of laser emission as  $\omega_0$  and introducing frequency deviation  $\Delta\omega(t)$  from  $\omega_0$ , we can write:  $\omega(t) = \omega_0 + \Delta\omega(t)$ , whence we get for the phase  $\varphi(t) = \varphi_p + \omega_0 t + \Delta\varphi(t)$ , where

$$\Delta\varphi(t) = \int_0^t \Delta\omega(t') dt'. \quad (5)$$

Given the above expressions for the phase, the intensity of a pair of interfering pulses can be written in the following form:

$$S(t) \sim \left| \sqrt{P_1(t)} \exp \left[ i\Delta\varphi(t) + i\varphi_{p1} + i\theta_1 \right] + \sqrt{P_2(t-\Delta t)} \exp \left[ i\Delta\varphi(t-\Delta t) + i\varphi_{p2} + i\theta_2 \right] \right|^2, \quad (6)$$

where it is taken into account that pulses acquire different phases when passing along different interferometer arms, such that  $\Delta\theta = \theta_2 - \theta_1 = 2\Delta L n \omega_0 / c$ , where  $n$  is the fiber refractive index. In addition, we introduced in Eq. (6) the inaccuracy of pulse overlap  $\Delta t$ , i.e. we took into account that one of the pulses may exit the interferometer a bit earlier than the other. We also used the identity  $|\exp(i\omega_0 t)|^2 = 1$ . It should be noted that the second term in Eq. (6) does not contain the factor  $\exp(i\omega_0 \Delta t)$  that reflects the fact that the phase difference of the pulses does not depend on the accuracy of their overlap, but is determined by their initial values at the laser output and by the interferometer delay line.

## 2.2 Chirp

Current modulation in gain-switched lasers causes a change of the carrier number  $N$ , which, in turn, leads to a change in the refractive index and, as a consequence, to a change in the laser frequency. As a result, optical frequency in the laser pulse is chirped. When neglecting

the spontaneous emission term and expanding the gain coefficient into the series near threshold, one can exclude explicit dependence on  $N$  from the rate equation for the phase. Using the relation  $d\varphi/dt = \omega(t) - \omega_0 = \Delta\omega(t)$  one can then rewrite this equation in the following form [12]:

$$\Delta\omega(t) = \frac{\alpha}{2} \left[ \frac{1}{P(t)} \frac{dP(t)}{dt} + k_a P(t) \right], \quad (7)$$

where  $\alpha$  is the linewidth enhancement factor (Henry factor [13]) and  $k_a$  is the adiabatic chirp coefficient. Equation (7) is extremely useful, since it allows determining the laser pulse chirp using just the time dependence of the output optical power  $P(t)$ . Substituting  $\Delta\omega(t)$  found with Eq. (7) into Eq. (5), one can calculate  $\Delta\varphi(t)$  needed for determination of the interference signal given by Eq. (6). Note that the adiabatic chirp coefficient  $k_a$  is related to the gain non-linearity and can be defined as follows:  $k_a = \chi/\tau_{ph}$ , where  $\chi$  is the gain compression coefficient [12] and  $\tau_{ph}$  is the photon lifetime in the laser cavity. Thereby, at low output power, when the non-linearity of the gain coefficient can be neglected, one can take into account only transient chirp.

### 2.3 Jitter

In a gain-switched laser,  $\Delta t$  introduced in Eq. (6) will exhibit significant fluctuations, i.e. there is a considerable jitter. The main source of the jitter here are the fluctuations of pump current pulse front (the intrinsic jitter of pump current pulses) and the fluctuations of its amplitude. The relation between the jitter and these fluctuations is defined by the delay  $t_d$  occurred between the application of the current pulse and the emission of light in gain-switched lasers. The delay  $t_d$  can be estimated using the well-known formula [14, 15]:

$$t_d = \tau_e \ln \left( \frac{I_{on} - I_b}{I_{on} - I_{th}} \right), \quad (8)$$

where  $\tau_e$  is the effective carrier lifetime in the active region of a laser,  $I_{on}$  is the pump current pulse value,  $I_b$  is the bias current, and  $I_{th}$  is the laser threshold current. (In such notation, the peak-to-peak value of the current modulation is  $I_p = I_{on} - I_b$ .) One can see from Eq. (8) that the fluctuations of  $I_{on}$  will cause the fluctuations of the turn-on delay  $t_d$ . The variance of the total jitter can be then estimated using following formula [9]:

$$\sigma_{\Delta t}^2 = \sigma_p^2 + \frac{\tau_e^2 (I_{th} - I_b)^2}{(I_{on} - I_b)^2 (I_{on} - I_{th})^2} \sigma_{I_{on}}^2, \quad (9)$$

where  $\sigma_p$  is the rms of the intrinsic jitter of current pulses, and  $\sigma_{I_{on}}$  is the rms of the injection current fluctuations.

### 2.4 Relaxation oscillations

In the general case, the shape of a laser pulse cannot be described analytically and should be determined numerically by solving laser rate equations. In some cases, the shape of the pulse can be estimated using approximate analytical solutions. Thus, one can show that when the injection current is modulated above threshold, the rising edge of the pulse is described by the Gaussian function [12]; therefore, Gaussian approximation for the pulse shape is often used in this case. In gain-switched lasers such an approximation is, strictly speaking, invalid; nevertheless, the Gaussian function is used as an approximation for bell-shaped narrow pulses even in this case. If the electric pulse is wide enough, then the laser pulse shape can be

distorted by transients, and the optical signal will contain spikes corresponding to relaxation oscillations. The angular frequency  $\omega_r$  of these oscillations can be estimated using small signal analysis [12]:

$$\omega_r = \sqrt{\frac{dG}{dN} \frac{I_{on} - I_{th}}{e} \frac{1}{\tau_{ph}}}, \quad (10)$$

where  $e$  is the absolute value of the electron charge,  $G$  is the normalized (dimensionless) gain coefficient and, as above,  $\tau_{ph}$  is the photon lifetime. Using Eqs. (8) and (10) one can estimate the critical width of the pump current pulse, at which the optical pulse will not be distorted yet by transients, i.e. at which the relaxation spikes will not have time to appear. It is obvious, that to avoid the appearance of relaxation oscillations, the electric signal should disappear after the onset of laser emission no later than half the period of the spikes. If the bias current is below threshold, then the maximum electric pulse width at which the optical pulse will have a bell-shaped (i.e. Gaussian) appearance can be written as  $T_p = t_d + \pi/\omega_r$ , where  $t_d$  is the turn-on delay defined by Eq. (8). Neglecting the non-linearity of the gain coefficient, i.e. assuming that  $G$  can be written as  $G = (N - N_0)/(N_{th} - N_0)$ , we will get for the derivative in (10):  $dG/dN = 1/(N_{th} - N_0)$ . One can then write  $T_p$  as follows:

$$T_p = \tau_e \ln \left( \frac{I_p}{I_p + I_b - I_{th}} \right) + \pi \sqrt{\tau_{ph} \tau_e} \sqrt{\frac{I_{th} - I_0}{I_p + I_b - I_{th}}}, \quad (11)$$

where we used relations:  $I_{on} = I_b + I_p$ ,  $I_{th} = eN_{th}/\tau_e$ , and  $I_0 = eN_0/\tau_e$ . (Here,  $N_0$  is the carrier number corresponding to the transparency of the laser material, and  $N_{th}$  is the threshold carrier number.) It is important to note that Eq. (11) is valid only for current pulses separated by the delay at least 4-5 times exceeding the effective carrier lifetime. In fact, Eq. (8) for  $t_d$  was derived under the assumption that before turning on the injection current,  $I_b \rightarrow I_{on}$ , the carrier number  $N$  has time to reach stationary value defined by the value of the bias current  $I_b$ . If, however, the time delay between current pulses is less than the carrier lifetime, Eq. (8) becomes invalid.

Let us modify Eq. (8) for the case, when the injection current  $I$  varies in time as a square wave with the pulse width of  $T_p$  and the inter-pulse delay of  $T_i$ . We will assume that after the time  $T_p$ , when the injection current changes from  $I_{on}$  to  $I_b$ , the carrier number is  $N \approx N_{th}$ . Let us use this assumption as an initial condition for the equation

$$\frac{dN}{dt} = \frac{I}{e} - \frac{N}{\tau_e} \quad (12)$$

defining the time dependence of the carrier number below threshold, i.e. let us put in Eq. (12)  $N(0) = N_{th}$  and  $I = I_b$ . We will have then for  $N$  at time  $t = T_i$ :

$$N(T_i) = \frac{I_b \tau_e}{e} + \exp \left( -\frac{T_i}{\tau_e} \right) \left[ N_{th} - \frac{I_b \tau_e}{e} \right]. \quad (13)$$

Let us again solve Eq. (12), but now using Eq. (13) as an initial condition for the carrier number and putting  $I = I_b + I_p$ . The time  $t_d'$  during which the carrier number will reach  $N_{th}$  is now defined as

$$t'_d = \tau_e \ln \left( \frac{I_b + I_p e^{T_i/\tau_e} - I_{th}}{I_b + I_p - I_{th}} \right) - T_i. \quad (14)$$

So, the maximum electric pulse width  $T_p$ , at which the relaxation spikes will not have time to appear should be defined more generally as  $T_p = t'_d + \pi/\omega_r$ , and Eq. (11) should be rewritten as follows:

$$T_p = \tau_e \ln \left( \frac{I_b + I_p e^{T_i/\tau_e} - I_{th}}{I_b + I_p - I_{th}} \right) - T_i + \pi \sqrt{\tau_{ph} \tau_e} \sqrt{\frac{I_{th} - I_0}{I_p + I_b - I_{th}}}. \quad (15)$$

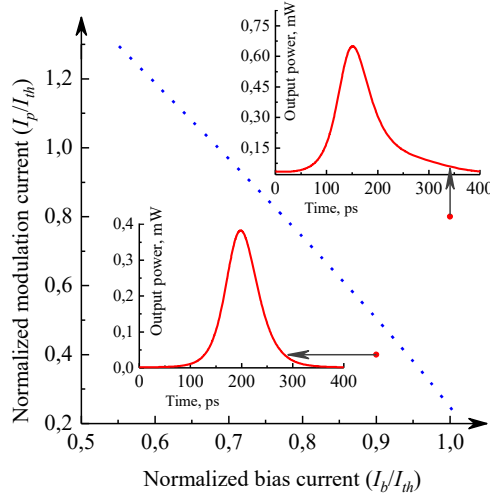


Fig. 2. Dashed line corresponds to the graphic solution of Eq. (15) (see details in the text). Optical signals found from the solution of laser rate equations for two different sets of  $(I_b, I_p)$  are shown in the insets.

Note that Eq. (8) can be considered as an extreme case of Eq. (14). It is easy to show that

$$\lim_{T_i \rightarrow \infty} t'_d = t_d. \quad (16)$$

Equation (15) can be considered as approximately valid also when the injection current varies harmonically:

$$I(t) = I_b + \frac{I_p}{2} [1 + \cos(\omega_p t)], \quad (17)$$

where  $\omega_p$  is the current modulation (angular) frequency. In this case, one should put  $T_p = T_i = \pi/\omega_p$ .

One can see from Eq. (15) that for a given time dependence of the injection current, i.e. at fixed values of  $T_p$ ,  $T_i$  or  $\omega_p$ , one can change the shape of the output laser pulse by varying values of  $I_p$  and  $I_b$ . To find a quantitative relationship between the values of currents  $I_p$ ,  $I_b$  and the shape of optical pulses, it is convenient to rewrite Eq. (15) in terms of dimensionless parameters  $y = I_p/I_{th}$  and  $x = I_b/I_{th}$  and consider it as an implicit function  $f(x, y) = 0$ . Dashed line in Fig. 2 corresponds to the graphic solution of Eq. (15) for the injection current having a form of a square wave with  $T_p = T_i = 200$  ps and the following

characteristic set of parameters:  $\tau_{ph} = 10$  ps,  $\tau_e = 1$  ns, and  $I_0 = 0.9I_{th}$ . In a sense, the resulting line represents some kind of a phase boundary, all points to the left of which correspond to the values of currents  $I_p$  and  $I_b$ , which do not distort the output laser pulse by relaxation oscillations. All points to the right of the dashed line in Fig. 2 correspond to the values of currents  $I_p$  and  $I_b$ , at which relaxation spikes appear in the optical signal.

To demonstrate pulse shapes corresponding to two different points  $(x, y)$  of the diagram, we show in the insets of Fig. 2 optical signals found from the solution of laser rate equations for two different sets of  $I_p$ ,  $I_b$ . For the simulation of laser pulses we used the same parameters as for the solution of Eq. (15), but the injection current was assumed to vary harmonically according to Eq. (17) with  $\omega_p/2\pi = 2.5$  GHz. Selected points are connected by arrows with corresponding pulses. Thus, it is clear that at the point  $(0.9, 0.4)$  the pulse has a Gaussian shape, whereas at the point  $(1, 0.8)$  the output optical power has a significant contribution from relaxation oscillations. (Note also the lower output power in the case of the Gaussian pulse.)

Thus, one should be careful when approximating a laser pulse shape with a Gaussian function. It is important to note that if the bandwidth of the photodetector or oscilloscope is small, the optical pulse can be so broadened that the relaxation spike will be hidden under its wings and the optical signal will look like a bell-shaped pulse. Therefore, when using a simplified model to describe the shape of a laser pulse, one should first make sure that values of  $I_p$  and  $I_b$  are chosen so that the corresponding point  $(x, y)$  is to the left of the line given by Eq. (15). Obviously, when the corresponding point  $(x, y)$  is to the right of this line, the Gaussian approximation cannot be used and the laser pulse shape should be found from the solution of rate equations.

### 3. Monte-Carlo simulations

#### 3.1 Preliminaries

Since phases of optical pulses emitted by the gain-switched laser in different moments of time are random, the intensity  $S(t)$  of the interference signal given by Eq. (6) is also random for different pairs of interfering pulses. From the experimental point of view, the source of randomness in the laser pulse-based QRNG [4, 16] is the interference signal  $S(t)$ ; therefore, its PDF is of fundamental importance. In order to simplify further analysis, it makes sense to get rid of the time dependence in  $S(t)$  considering instead the integral signal:

$$\tilde{S} = \frac{\int_{-T/2}^{T/2} S(t) dt}{\int_{-T/2}^{T/2} P_1(t) dt}, \quad (18)$$

where  $T$  is a time window cutting out a separate pulse from the pulse train, and normalization is performed with respect to the pulse exiting from the short arm of the interferometer. Assuming that the interference of a given pair of pulses does not affect the interference of the next pair of pulses, one can put  $T \rightarrow \infty$  in Eq. (18). A further problem is then reduced to finding the PDF of the integral signal  $\tilde{S}$ . Note that even in the simplest model with Gaussian pulses without chirp this problem cannot be solved analytically, since  $\tilde{S}$  depends on several random variables.

The principal random variable here is the laser pulse phase  $\varphi_p$ . One can show that fluctuations of  $\varphi_p$  exhibit normal PDF with an rms  $\sigma_\varphi$  defined by the rate of radiative spontaneous recombination [17]. Since  $\varphi_p$  stands in the argument of the exponent in Eq. (6), its fluctuations can be considered completely random when  $\sigma_\varphi > 2\pi/\sqrt{2}$  (see appendix in [18] for details). (This condition can be reformulated in terms of the phase difference  $\Delta\Phi = \varphi_{p_2} - \varphi_{p_1} + \theta_2 - \theta_1$  as follows: fluctuations of  $\Delta\Phi$  can be considered completely random when  $\sigma_{\Delta\Phi} = \sqrt{2}\sigma_\varphi > 2\pi$ .) In fact, if  $\sigma_\varphi$  obeys this inequality, the PDF of laser phase fluctuations can be well approximated by a uniform distribution in the interval  $(0, \pi]$ . In [16], fluctuations of the laser pulse phase  $\sigma_\varphi$  were estimated experimentally for the gain-switched laser operating at an amplitude modulation frequency of 5.825 GHz, and was shown to be  $\sigma_\varphi > 9.45$ . At lower pulse repetition rate it should become even easier to meet the requirement  $\sigma_\varphi > 2\pi/\sqrt{2}$ .

Another random variable in Eq. (6) is the inaccuracy of the pulse overlap  $\Delta t$ , which fluctuates due to jitter. As mentioned above, in gain-switched lasers the jitter is mainly caused by fluctuations of the injection current, which lead to fluctuations of the turn-on delay  $t_d$  defined by Eq. (8) (or rather by Eq. (14)). Assuming that fluctuations of  $I_{on}$  (or  $I_p$ ) exhibit normal PDF, one can show that PDF of  $t_d$  is asymmetric. Nevertheless, taking into account the intrinsic jitter of current pulses one can assume with a good accuracy that fluctuations of  $\Delta t$  exhibit normal PDF with a variance given by Eq. (9).

Based on the above reasoning about the relationship between the injection current parameters and the shape of optical signal, it is obvious that current fluctuations will lead not only to the jitter, but also to random changes in the output optical power  $P(t)$ . If the pump current fluctuations are relatively small, one can neglect the change in the pulse shape and assume that only the “area” under the pulse is fluctuating. In this case, the output power for the  $i$ -th pulse ( $i=1,2$ ) can be written as  $a_i P_i(t)$ , where  $a_i$  is a random variable with the mean value equal to  $\bar{a} = 1$  and the PDF  $f_a$  defining the relationship between fluctuations of the injection current and  $P(t)$ . We will assume for simplicity that  $f_a$  has the form of normal distribution with the rms of  $\sigma_a$ . It is important to note that although introduced random variables  $a_i$  have the same mean value and exhibit equivalent PDFs with the same rms value, they cannot be substituted by a single random variable  $a$ , since fluctuations of  $P_1(t)$  and  $P_2(t)$  are independent.

The PDF of the integral signal  $\tilde{S}$  is defined by the derivative:  $f_{\tilde{S}} = F'_{\tilde{S}}$ , where, by definition, the cumulative distribution function  $F_{\tilde{S}}$  is determined by integrating the joint PDF of all fluctuating quantities in  $\tilde{S}$  [19]. Assuming that fluctuations of  $\varphi_{p_1}$ ,  $\varphi_{p_1}$ ,  $a_1$ ,  $a_2$ , and  $\Delta t$  are independent the joint PDF represents just a product of all corresponding PDFs:  $f_{\varphi_{p_1}} f_{\varphi_{p_1}} f_{a_1} f_{a_2} f_{\Delta t}$ . The integration area, in turn, is defined by the inequality  $\tilde{S} < y$ , where  $\tilde{S}$  means the functional dependence of  $\tilde{S}$  on  $\varphi_{p_1}$ ,  $\varphi_{p_1}$ ,  $a_1$ ,  $a_2$ , and  $\Delta t$ . Unfortunately,  $F_{\tilde{S}}$  cannot be calculated analytically; therefore, Monte-Carlo simulation is often used even for simple models.

In a real experiment, the PDF of the interference signal is additionally “broadened” due to noises in the photodetector. Moreover, the PDF can be shifted due to the “flare” arising from

reflections in optical elements of the interference scheme. The experimental signal should be therefore written as follows:

$$\tilde{S} \rightarrow \tilde{S} + \zeta, \quad (19)$$

where  $\zeta$  is the noise signal, whose probability distribution is generally considered to be Gaussian.

Note that  $f_{\tilde{S}}$  depends not only on the constituent PDFs, but also on the integration area, which is defined by the functional form of  $\tilde{S}$ . The latter, in turn, is determined by the shape of laser pulses  $P(t)$  and by the chirp  $\Delta\omega(t)$ . Therefore, it seems useful to consider the dependence of  $f_{\tilde{S}}$  on  $P(t)$  and  $\Delta\omega(t)$ . We consider here five different models (see Fig. 3), gradually increasing their complexity.

### 3.2 Gaussian pulse without chirp

First, let us obtain the expression for  $\tilde{S}$  in the case, when the shape of the laser pulse is defined by the Gaussian function:

$$P_i(t) = P_{0i} \exp\left(-\frac{t^2}{2w^2}\right), \quad (20)$$

where  $w$  is the rms width of the pulse (the full width at half maximum is defined as  $w_{FWHM} = 2w\sqrt{2\ln 2} \approx 2.35w$ ) and  $P_{0i}$  is a peak power value of the  $i$ -th pulse at the output of the interferometer (recall that the subscript  $i=1,2$  distinguishes the arms of the interferometer).

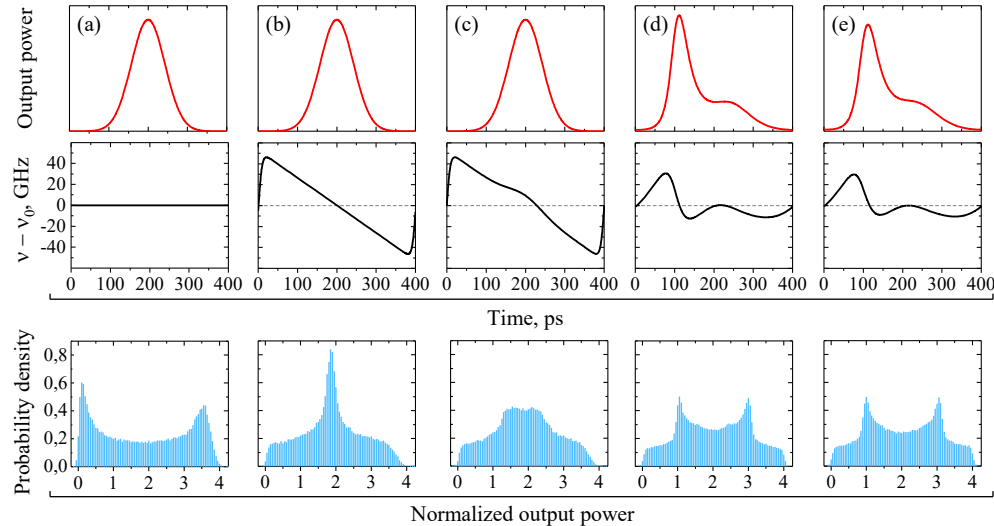


Fig. 3. The shape of the laser pulse (top), its chirp according to Eq. (7) (middle) and the PDF of the normalized interference signal (bottom) in different models: (a) Gaussian laser pulse without chirp; (b) Gaussian laser pulse with transient chirp; (c) Gaussian laser pulse with transient and adiabatic chirp; (d) non-Gaussian laser pulse with transient chirp; (e) non-Gaussian laser pulse with transient and adiabatic chirp. The pulse repetition rate in all models was assumed to be 2.5 GHz; the rms width of the Gaussian pulses in models (a), (b), and (c) was put to 100 ps; the linewidth enhancement factor was put to 6 everywhere except model (a), where it was put to 0; in models (c) and (e), the adiabatic chirp coefficient was put to  $k_a = 5$  THz/W. Laser pulse simulation parameters used in the models (d) and (e) were:

$$\tau_{ph} = 10 \text{ ps}, \tau_e = 1 \text{ ns}, N_0 = 4.8 \times 10^7, N_{ph} = 5.3 \times 10^7, I_b = 9 \text{ mA}, I_p = 14 \text{ mA}, \varepsilon = 0.15, \Gamma = 0.15, C_{sp} = 10^{-5}.$$

In the absence of chirp, the phase  $\Delta\phi(t)$  in Eq. (6) equals to zero; therefore, integrating and normalizing the signal  $S(t)$  according to Eq. (18) we have:

$$\tilde{S} = s_1 + s_2 + 2\eta_{\Delta t} \sqrt{s_1 s_2} \cos \Delta\Phi, \quad (21)$$

where  $s_1$  and  $s_2$  are normalized integral signals exiting from the short and long arms of the interferometer, respectively,  $\Delta\Phi = \Delta\phi_p + \Delta\theta$  is the phase difference of interfering pulses, and the visibility  $\eta_{\Delta t}$  is defined as follows:

$$\eta_{\Delta t} = e^{-\frac{\Delta t^2}{8w^2}}. \quad (22)$$

Normalized signals  $s_i$  are related to random variables  $a_i$  introduced above in the following way:  $s_1 = a_1$  and  $s_2 = r a_2$ , where

$$r = \frac{(1-\alpha_2)T_{02}T_{20}}{(1-\alpha_1)T_{01}T_{10}}. \quad (23)$$

The shape of the laser pulse, its chirp and the PDF of the normalized interference signal corresponding to this simple model are shown in Fig. 3(a). For Monte-Carlo simulations, we used Eq. (21) assuming that variables  $\Delta\Phi$ ,  $\Delta t$ ,  $s_1$ , and  $s_2$  exhibit normal distribution with the following rms values:  $\sigma_{\Delta\Phi} = 2\pi$ ,  $\sigma_{\Delta t} = 20 \text{ ps}$ , and  $\sigma_s = \sigma_a = 0.05$ . In addition, we took into account the photodetector voltage fluctuations according to Eq. (19), assuming that they correspond to the Gaussian noise with the zero mean value and the rms value of 0.05. The quantity  $r$  from Eq. (23) was taken to be 0.85, i.e. we assumed that losses in the long arm of the interferometer are significantly higher than in the short one. One can see from Fig. 3(a) that the PDF exhibits noticeable asymmetry: the left maximum is much higher and “thinner” than the right one. This feature is due to fluctuations of normalized amplitudes  $s_1$  and  $s_2$  and it becomes more pronounced when increasing the rms value of these fluctuations. Note also that the jitter  $\Delta t$  mean value was put to zero in Fig. 3(a). If, however, its mean value is different from zero, then the mean value of the  $\exp(-\Delta t^2/8w^2)$  term in Eq. (21) will be different from unity, which will reduce the visibility of the interference.

### 3.3 Gaussian pulse with transient chirp

The picture is much more complicated, if the frequency modulation is taken into account. To find  $\Delta\phi(t)$ , substitute Eq. (20) into Eq. (7) and integrate the result over time. Assuming that the adiabatic chirp coefficient is zero:  $k_a = 0$ , we get:

$$\Delta\phi(t) = -\frac{\alpha}{4w^2} t^2. \quad (24)$$

Thus, in the absence of the gain non-linearity, the Gaussian optical pulse is down-chirped (see Fig. 3(b)) and its chirp is linear:  $\Delta\omega(t) = -\beta t$ , where  $\beta$  is the linear chirp coefficient defined by  $\beta = \alpha/2w^2$ . The result of the interference, i.e. the  $S(t)$  function, is more complex in this case, since the cosine argument in the interference term depends now on time and on  $\Delta t$ . However, the dependence on  $\Delta t$  disappears when integrating the signal according to Eq. (18), and we again obtain Eq. (21) for  $\tilde{S}$ , but with the visibility defined by

$$\eta_{\Delta t} = e^{-\frac{(1+\alpha^2)\Delta t^2}{8w^2}}. \quad (25)$$

According to Eq. (25), the linear chirp increases the jitter effect by a factor  $\sqrt{1+\alpha^2}$ , which is clearly manifested in a change of the PDF appearance shown in Fig. 3(b), where one can see the high peak in the center. This peak indicates an increase in the probability that the signal equals to  $\tilde{S} = s_1 + s_2$ , which is the evidence of interference worsening. Simulation parameters in Fig. 3(b) were the same as in the previous model; the linewidth enhancement factor  $\alpha$  was put to 6.

It is important to note that if the mean value of  $\Delta t$  is zero, than  $\eta_{\Delta t}$  in both models (Eqs. (22) and (25)) equals to unity, i.e., in terms of visibility, interference does not deteriorate when adding linear chirp to the model. Indeed, although  $\Delta t$  and  $\Delta\Phi$  in Eq. (21) have different values for different pairs of interfering pulses, there is a fairly high probability that the instant value of  $\Delta t$  will be zero and simultaneously  $\Delta\Phi = \pi$  (which provides perfect destructive interference) or  $\Delta\Phi = 0$  (which provides perfect constructive interference). However, the joint probability of these events decreases when increasing jitter, which leads to an increase in the central peak in the PDF of the integral signal  $\tilde{S}$ . Therefore, speaking about the deterioration of interference, we do not mean a decrease in visibility but the deviation of the signal PDF from that shown in Fig. 3(a).

### 3.4 Gaussian pulse with transient and adiabatic chirp

If we consider also the adiabatic chirp, then the phase  $\Delta\phi(t)$  will have the following form:

$$\Delta\phi(t) = -\frac{\alpha}{4w^2}t^2 + \frac{\alpha w\sqrt{2\pi}}{4}k_a P_0 \operatorname{erf}\left(\frac{t}{w\sqrt{2}}\right). \quad (26)$$

Unfortunately, the analytical expression for the interference signal  $\tilde{S}$  cannot be obtained in this case; therefore, the PDF simulation has to be performed numerically with Eq. (6). Calculated PDF of the signal  $\tilde{S}$  is shown in Fig. 3(c), where we used  $k_a = 5$  THz/W and  $P_0 = 4$  mW (all other simulation parameters were the same as in the previous models). One can see that in the presence of the adiabatic chirp, the central maximum splits into two peaks, i.e. non-linearity of the chirp leads to a decrease of the probability that the signal equals to  $\tilde{S} = s_1 + s_2$ . Thus, oddly enough, the PDF of the interference signal becomes more uniform in the presence of the adiabatic chirp, so, in a statistical sense, the interference improves. It is interesting that when increasing the adiabatic chirp coefficient  $k_a$ , the “distance” between these peaks increases (at least up to a certain value of  $k_a$ ).

### 3.5 Non-Gaussian pulse

Finally, we consider a more general case when the optical pulse cannot be described by the Gaussian function and one should use laser rate equations to find the shape of the output signal. We will consider here the case when the laser pulse shape is affected by only the first relaxation spike. When solving the rate equations, we used the following values for the lifetimes:  $\tau_{ph} = 2$  ps and  $\tau_e = 0.5$  ns; the threshold current  $I_{th}$  was put to 10 mA and it was assumed that the injection current varies according to Eq. (17) with  $\omega_p/2\pi = 2.5$  GHz and  $I_p = 10$  mA,  $I_b = 8$  mA. The case, when the gain compression coefficient  $\chi$  (and consequently the adiabatic chirp coefficient  $k_a = \chi/\tau_{ph}$ ) is zero is shown in Fig. 3(d). Figure 3(e), in turn, demonstrates the case when the compression gain coefficient is

$\chi = 10 \text{ W}^{-1}$ , which corresponds to  $k_a = 5 \text{ THz/W}$ . The differential quantum output was  $\varepsilon = 0.11$ . (Other simulation parameters were the same as in the previous models.)

One can see that due to the asymmetry of the output power  $P(t)$ , the chirp  $\Delta\omega(t)$  has a quite complicated form even in the absence of the adiabatic term. The PDF of the interference signal in Fig. 3(d) exhibits two pronounced maxima, which, in contrast to Fig. 3(a), do not correspond to an ideal constructive and destructive interference. Note that the PDF in Fig. 3(d) is somewhat similar to that shown in Fig. 3(c), where the splitting of the PDF's maximum is related to the chirp non-linearity. However, the difference between Fig. 3(c) and Fig. 3(d) is that the chirp non-linearity in the latter case is caused by the relaxation oscillations and not by the adiabatic term. It is for this reason the inclusion of the adiabatic chirp into the non-Gaussian pulse does not lead to a significant change in the PDF, as it is seen from the comparison of Figs. 3(d) and 3(e).

## 4. Experiments

### 4.1 Experimental setup

The optical scheme used in this work to observe interference of laser pulses is shown in Fig. 1. Unbalanced fiber optic Michelson interferometer was built using an optical circulator, a 50:50 single mode (SM) fiber coupler, SM fiber patch cable as a delay line, and two Faraday mirrors used to compensate the effects of polarization mode dispersion in SM fiber components. The length of the delay line  $\Delta L$  was calculated using the following formula:

$$2\Delta L = \frac{2\pi N_p c}{\omega_p n_g}, \quad (27)$$

where  $c$  is the speed of light in vacuum,  $n_g$  is the group index,  $\omega_p$  is the current modulation (angular) frequency corresponding to the pulse repetition rate, and  $N_p$  is the number of pulses emitted by the laser during the time when the given pulse travels the distance  $2\Delta L$  (the factor 2 before  $\Delta L$  takes into account the fact that the pulse passes two times through the delay line in the Michelson interferometer). In our case,  $\Delta L$  was 128 cm, which at  $\omega_p/2\pi = 2.5 \text{ GHz}$  provides  $N_p = 32$ , such that the first laser pulse interferes with the 33<sup>rd</sup> one, the second pulse interferes with the 34<sup>th</sup> one, etc.

The 1550 nm telecom distributed feedback (DFB) laser with 10 Gbps modulation bandwidth was driven by a commercial 11.3 Gbps low-power laser diode driver. Thermal stabilization of the laser diode was performed using Peltier thermoelectric cooler controlled by commercially available single-chip temperature controller. The waveform modulated at 2.5 GHz was generated by a phase-locked loops multiplying the input frequency from the 10 MHz reference oscillator. The peak-to-peak value of the modulation current  $I_p$  was estimated to be  $\sim 10 \text{ mA}$ . The laser threshold current  $I_{th}$  found from the light-current characteristics was estimated to be around 9 mA.

To detect the optical output we used the home-built photodetector equipped by a p-i-n photodiode with 10 GHz bandwidth. The signal processing was performed using the Teledyne Lecroy digital oscilloscope (WaveMaster 808Zi-A) with 8 GHz bandwidth and temporal resolution of 25 ps. Optical spectra were acquired using Thorlabs optical spectrum analyzer (OSA 202) with a spectral resolution of 7.5 GHz.

### 4.2 Experimental results

Experimental PDFs of the interference signal at four different values of the bias current  $I_b$  are shown in Fig. 4 by red circles. Corresponding simulations are shown by blue histograms. According to the theoretical consideration given above (see Fig. 2), the contribution of

relaxation oscillations at  $I_b = 6$  mA is quite small, such that the experimental laser pulse shape (not shown here) could be approximated by the Gaussian function. Moreover, one can neglect the adiabatic chirp due to the small output power. Therefore, the corresponding PDF is similar to that shown in Fig. 3(b). Note, however, that for more generality we performed the simulations shown in Fig. 4 with the use of Eqs. (6) and (7). We put  $\alpha = 6$  for the Henry factor, whereas the rms values of the jitter and normalized power fluctuations were put  $\sigma_{\Delta t} = 20$  ps and  $\sigma_a = 0.05$ , respectively. Initial phases of laser pulses were assumed to exhibit normal distribution with  $\sigma_\phi = 2\pi$ . (Note that we obtained almost identical PDF for  $I_b = 6$  mA with Eq. (21).) Other parameters used for the laser pulse simulation were:  $\tau_{ph} = 15$  ps,  $\tau_e = 1.1$  ns,  $\chi = 10$  W<sup>-1</sup>,  $N_0 = 4.8 \times 10^7$ ,  $N_{th} = 5.3 \times 10^7$ ,  $I_p = 10$  mA,  $\varepsilon = 0.15$ . (The differential quantum output was estimated experimentally from the laser light-current characteristic.)

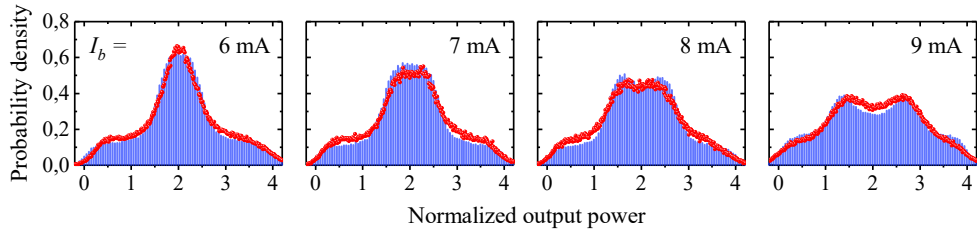


Fig. 4. Experimental PDFs of the interference signal at four different values of the bias current  $I_b$  (red circles) and corresponding Monte-Carlo simulations (histograms). The peak-to-peak value of the modulation current was  $\sim 10$  mA in all cases.

The PDF at  $I_b = 9$  mA is substantially different from that obtained at  $I_b = 6$  mA in accordance to theoretical predictions: the higher value of the bias current provides the higher impact of relaxation oscillations (see Fig. 2). Moreover, the higher output power does not allow neglecting the adiabatic chirp, so the model given by Fig. 3(e) should be used in this case. Two intermediate PDFs in Fig. 4 are presented to demonstrate its evolution from lower to higher values of the bias current.

Obviously, the “chirp + jitter” effect can be reduced by either reducing jitter or chirp, or both. In our opinion, the simplest (and cheapest) solution is to use the bandpass filter to cut off a part of the laser spectrum associated with chirp. In the case of the Gaussian laser pulse with linear chirp, this approach would be more difficult, since it is necessary to cut off both the high- and low-frequency components of the spectrum. For the non-Gaussian pulse affected by relaxation oscillations, the optical spectrum will have essential asymmetry, since only the rising edge of the laser pulse will be chirped significantly. One can see from Fig. 3(e) that when the relaxation spike occurs, the absolute value of  $\Delta\omega$  decreases, which makes the falling edge of the pulse less chirped. Therefore, it is enough just to cut off the high-frequency part of the spectrum in this case.

To cut off the laser spectrum we used the telecom dense wavelength division multiplexing (DWDM) filter with 100 GHz bandwidth placed just after the laser output (see Fig. 1). The position of the laser spectrum on the frequency axis was adjusted by changing the laser temperature in such a way that the high-frequency shoulder was beyond the filter bandwidth. Experimental optical spectra at  $I_b = 9$  mA without and with DWDM filter are shown in Fig. 5(a) by empty triangles and empty circles, respectively. The central frequency  $\nu_0$  corresponds to the filtered spectrum “center of gravity” at given temperature and is  $\nu_0 = 193.63$  THz. One can see that the unfiltered spectrum has a broad high-frequency shoulder, which is apparently related to the laser pulse chirp. Indeed, the corresponding PDF

shown in Fig. 5(b) by filled triangles exhibits the specific shape caused by the interference of chirped non-Gaussian laser pulses. The PDF obtained with the DWDM filter (filled circles in Fig. 5(b)) exhibits two pronounced maxima corresponding to the constructive and destructive interference, as for the model shown in Fig. 3(a).

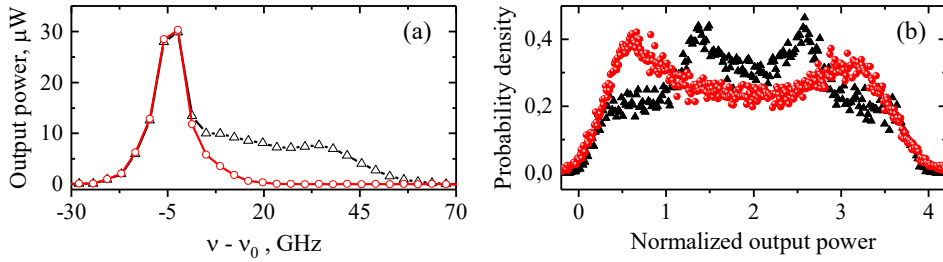


Fig. 5. (a) Experimental optical spectra at  $I_b = 9$  mA without (empty triangles) and with (empty circles) DWDM filter. (b) Experimental PDFs of the interference signal at  $I_b = 9$  mA without (filled triangles) and with (filled circles) DWDM filter.

It should be noted here that the spectral filtering does not change the chirp itself, but changes the intensity distribution of spectral components in the pulse. In fact, we observed a decrease in the intensity of the rising edge of the laser pulse after passing the optical filter, which is caused by the fact that its rising edge is chirped more significantly than the falling one. So, an optical filter in a sense improves spectral matching of the pulses improving thus their interference.

### Conclusions

We demonstrated that chirp, jitter and relaxation oscillations have a significant impact on the interference of laser pulses. We derived a simple estimate (Eq. (15)) for the contribution of relaxation oscillations, which provides the quantitative evaluation of applicability of the Gaussian approximation for the laser pulse shape. It was shown that the relaxation spike makes the falling edge of the laser pulse less chirped and thus reduces the impact of the “chirp + jitter” effect on the appearance of the signal PDF. Moreover, the optical spectrum of the chirped pulse accompanied by relaxation oscillations exhibits significant asymmetry and can be easily cut off with a bandpass filter.

In the context of a QRNG, the jitter should be considered as a source of a “classical” noise, since it is mainly caused by fluctuations of the pump current. Quantum noise originating in spontaneous emission and amplified via the pulse interference is thus “contaminated” by the jitter. Therefore, the combined effect of the chirp and jitter is crucial when elaborating QRNG and must be minimized. This is the main imperative to use the bandpass optical filter in the interference scheme under consideration.

It is important to note that jitter is not the only source of classical noise and other “non-quantum” fluctuations should be taken into account. This issue will not be considered in the present paper, since it requires a lot of space and will be presented in a separate article. In the related paper [18], we will try to draw a clear line between quantum and classical fluctuations and provide a method to extract pure quantum noise from the interference of laser pulses.

### Appendix

The laser pulse shapes used in the main text were found using the following system of rate equations for the photon number  $Q$  and the carrier number  $N$  [12, 20, 21]:

$$\begin{aligned}\frac{dQ}{dt} &= \left( \frac{N - N_0}{N_{th} - N_0} (1 - \chi_Q Q) - 1 \right) \frac{Q}{\tau_{ph}} + C_{sp} \frac{N}{\tau_e}, \\ \frac{dN}{dt} &= \frac{I}{e} - \frac{N}{\tau_e} - \frac{Q}{\Gamma \tau_{ph}} \frac{N - N_0}{N_{th} - N_0} (1 - \chi_Q Q),\end{aligned}\quad (\text{A.1})$$

where  $N_{th}$  and  $N_0$  are the carrier numbers at threshold and transparency, respectively;  $\tau_{ph}$  and  $\tau_e$  are the effective lifetimes of photons and electrons in the active layer, respectively;  $I$  is the injection current,  $\Gamma$  is the confinement factor,  $\chi_Q$  is the dimensionless gain compression coefficient, and the factor  $C_{sp}$  corresponds to the fraction of spontaneously emitted photons that end up in the active mode under consideration. The relation between the number of photons and emitted optical power was defined as follows:

$$P = \frac{\varepsilon \hbar \omega_0}{2 \tau_{ph}} Q, \quad (\text{A.2})$$

where  $\hbar \omega_0$  is the photon energy,  $\varepsilon$  is the differential quantum efficiency, and the factor 1/2 takes into account that the output power is generally measured from only one facet. The gain compression coefficient is given by

$$\chi = \frac{2 \tau_{ph}}{\varepsilon \hbar \omega_0} \chi_Q. \quad (\text{A.3})$$

Everywhere in the main text, we used  $\Gamma = 0.15$ ,  $C_{sp} = 10^{-5}$ , and  $\omega_0/2\pi = 1.9363 \times 10^{14}$  Hz.

## Acknowledgments

The authors are grateful to Aleksey Fedorov and Denis Sych for valuable comments.

## Funding

Russian Science Foundation (Grant No. 17-71-20146)

## Disclosures

The authors declare no conflicts of interest

## References

1. H. Guo, W. Tang, Y. Liu, and W. Wei, "Truly random number generation based on measurement of phase noise of a laser," *Phys. Rev. E* **81**(5), 051137 (2010).
2. B. Qi, Y.-M. Chi, H.-K. Lo, and L. Qian, "High-speed quantum random number generation by measuring phase noise of a single-mode laser," *Opt. Lett.* **35**(3), 312-314 (2010).
3. C. R. S. Williams, J. C. Salevan, X. Li, R. Roy, and T. E. Murphy, "Fast physical random number generator using amplified spontaneous emission," *Opt. Express* **18**(23), 23584-23597 (2010).
4. M. Jofre, M. Curty, F. Steinlechner, G. Anzolin, J. P. Torres, M. W. Mitchell, and V. Pruneri, "True random numbers from amplified quantum vacuum," *Opt. Express* **19**(21), 20665-20672 (2011).
5. T. Symul, S. M. Assad, and P. K. Lam, "Real time demonstration of high bitrate quantum random number generation with coherent laser light," *Appl. Phys. Lett.* **98**(23), 231103 (2011).
6. J. Yang, J. Liu, Q. Su, Z. Li, F. Fan, B. Xu, and H. Guo, "5.4 Gbps real time quantum random number generator with simple implementation," *Opt. Express* **24**(24), 27475-27481 (2016).
7. P. Li, Y. Guo, Y. Guo, Y. Fan, X. Guo, X. Liu, K. Li, K. A. Shore, Y. Wang, and A. Wang, "Ultrafast Fully Photonic Random Bit Generator," *J. Lightwave Technol.* **36**(12), 2531-2540 (2018).
8. Z. L. Yuan, M. Lucamarini, J. F. Dynes, B. Fröhlich, A. Plews, and A. J. Shields, "Robust random number generation using steady-state emission of gain-switched laser diodes," *Appl. Phys. Lett.* **104**(26), 261112 (2014).
9. Z. Fang, H. Cai, G. Chen, and R. Qu, *Single Frequency Semiconductor Lasers* (Springer Nature, 2017).
10. E. H. Böttcher, K. Ketterer, and D. Bimberg, "Turn-on delay time fluctuations in gain-switched AlGaAs/GaAs multiple-quantum-well lasers," *J. Appl. Phys.* **63**(7), 2469-2471 (1988).
11. M. M. Choy, P. L. Liu, P. W. Shumate, T. P. Lee, and S. Tsuji, "Measurements of dynamic photon fluctuations in a directly modulated 1.5-μm InGaAsP distributed feedback laser," *Appl. Phys. Lett.* **47**(5), 448-450 (1985).

12. K. Petermann, *Laser Diode Modulation and Noise* (Kluwer Academic Publishers, 1988).
13. C. Henry, "Theory of the linewidth of semiconductor lasers," *IEEE J. Quantum. Elect.* **18**(2), 259-264 (1982).
14. K. Konnerth, and C. Lanza, "Delay between current pulse and light emission of a gallium arsenide injection laser," *Appl. Phys. Lett.* **4**(7), 120-121 (1964).
15. J. C. Dymont, J. E. Ripper, and T. P. Lee, "Measurement and Interpretation of Long Spontaneous Lifetimes in Double Heterostructure Lasers," *J. Appl. Phys.* **43**(2), 452-457 (1972).
16. C. Abellán, W. Amaya, M. Jofre, M. Curty, A. Acín, J. Capmany, V. Pruneri, and M. W. Mitchell, "Ultra-fast quantum randomness generation by accelerated phase diffusion in a pulsed laser diode," *Opt. Express* **22**(2), 1645-1654 (2014).
17. C. Henry, "Phase noise in semiconductor lasers," *J. Lightwave Technol.* **4**(3), 298-311 (1986).
18. R. Shakhovoy, D. Sych, V. Sharoglavova, A. Udaltssov, A. Fedorov, and Y. Kurochkin, "Quantum noise extraction from the interference of laser pulses in optical quantum random number generator," to be published
19. V. S. Pugachev, *Probability Theory and Mathematical Statistics for Engineers* (Oxford University, 1984).
20. G. P. Agrawal, and N. K. Dutta, *Semiconductor lasers* (Kluwer Academic Publishers, 1993).
21. G. H. M. v. Tartwijk, and D. Lenstra, "Semiconductor lasers with optical injection and feedback," *Quantum and Semiclassical Optics: Journal of the European Optical Society Part B* **7**(2), 87-143 (1995).